SUBSONIC INVESTIGATIONS ON CONFIGURATIONS WITH FORWARD- AND AFT-SWEPT WINGS OF HIGH ASPECT RATIO

R. K. Nangia
Consulting Engineer
SAC Technology Group, Bristol, UK

ABSTRACT

The idea of using Forward Swept Wing (FSW) is now being explored on several types of military and civil/transport aircraft. Most of the recent work is however connected with moderate aspect ratio configuration typified by the Grumman X-29 Advanced Technology FSW demonstrator. This paper relates to subsonic longitudinal tests and analysis carried out on two series of configurations with wings of aspect ratio near 8 - the aim being to gain an understanding of the FSW technology in the high aspect ratio range.

The first series represents the high-wing "Transport" types and the second, "Executive" types. In each series of models, Forward- and Aft-swept wings could be incorporated with the sweep angle reversed about 1/4 chord. Canard and high tail could also be represented. The comparable models had lifting surfaces of equivalent "gross" area but not equivalent "trimming" volume ratio. The FSW "Executive" type features a mid-wing location behind the passenger cabin. With the conventional Aft Swept Wing (ASW) "Executive" type, the wing is set low under the cabin.

An idea of aerodynamics of 3-surface layouts was also obtained. Tests included the effects of winglets, leading and trailing edge flaps and wing fences.

The results show that in spite of low test Reynolds No. (0.2×10^6 based on mean wing chord), several important conclusions can be drawn, eg.

(1) Gentler stall and improved high lift characteristics for the FSW configurations. Wing root design is important.

(2) Peak lift/drag ratio for the configurations occurred near C_L=0.6 (ie. in the "linear" range and before Reynolds number and flow separation effects dominate). Compared with the equivalent ASW + tail configurations, the FSW + canard configuration produced about 15 - 20% higher L/D (exact value depended on presence of winglets, wing fences, etc.).

(3) Winglets appeared to be 3 - 4 times more effective on FSW than on ASW (in lift, L/D terms). They also aid the dihedral stability of the FSW.

(4) Leading edge flaps were effective in delaying the FSW root flow separation.

The tests have made the case for further work on FSW's at higher subsonic and transonic Reynolds No. Lateral stability tests are also required. FSW configuration optimisation can be attempted by several means eg. by exploiting the reduced wing root bending moment extensive natural laminar boundary layer, the use of 3- surface concepts, etc.

NOMENCLATURE

A	gross Aspect ratio
b	span
c	chord
c_r	root chord at the centre-line
c_t	tip chord
$\bar{c}$	= $(c_r+c_t)/2$, geometric mean chord
$\bar{\bar{c}}$	aerodynamic mean chord
C_D	= D/(qS), drag coefficient
C_{DO}	C_D at C_L = 0
C_L	= L/(qS), lift coefficient
C_{Lmax}	peak C_L
C_{LL}	spanwise local lift
C_{LLmax}	peak of C_{LL}
ΔC_L	incremental C_L
C_m	= m/(qSc), pitching moment coefficient about defined axis
C_{mo}	pitching moment coefficient at C_L=0
D	drag force
i_w	wing root incidence
L	lift force
L.E.	Leading Edge
m	pitching moment about defined axis
q	= $\frac{1}{2}\rho V^2$ dynamic pressure
R	Reynolds No.
s	semi-span
S	gross wing area
S_c	gross canard area
S_T	gross tailplane area
T.E.	Trailing Edge
V	air velocity
x,y,z	Cartesian co-ordinate system, x-axis along fuselage
x_{ac}	chordwise position of aerodynamic centre or neutral point
y_{cp}	spanwise position of centre of load
y_L	position of peak C_{LL}
ρ	density of air
α	angle of attack from fuselage axis
Λ	sweep angle, +ve for sweep-back, -ve for sweep forward
δ_c	canard deflection (from fuselage axis)
δ_T	tailplane deflection(" " ")
η	= y/s, non-dimensional spanwise co-ordinate

I. INTRODUCTION

Some of the benefits of using Forward Swept Wing (FSW) on aircraft eg. lower lift induced drag and improved high angle of attack performance, have been appreciated for a number of years.

The lack of adequate structural technology in the past, to cope with the FSW aero-elastic divergence problem prevented a full exploitation of these benefits. With the recent advances, notably in composite material structures and improved understanding of flight dynamics and control, the idea of using FSW is being explored on several military and civil/ transport aircraft.

Wing sweep either aft or forward delays the transonic drag divergence by producing weaker oblique wing shock waves at a given lift. To overcome the FSW aero-elastic divergence tendency, the designer working in conventional isotropic materials required a stiffer and heavier wing structure with associated design penalties. The penalties grew with increasing forward sweep. This design obstacle for FSW channelled the major effort in technology towards Aft Swept Wing (ASW) aircraft.

Early German work led to the appearance of a FSW on the Junkers JU-287 which first flew in 1944 (Fig. 1). The FSW allowed the design of a large bomb bay with the store suspended on the aircraft's c.g. The JU-287 flew about 16 times before the close of World War II. The FSW re-appeared in 1964 on the HFB 320 Hansa Jet (Fig. 2). Forward sweep in this case allowed the main spar to be located aft of the passenger cabin (Ref. 1). Both the above aircraft had relatively low wing sweep angle where the divergence problem is not severe. Both used tail stabilizers.

The configuration optimisation programme of the Hansa included several design variables (Ref. 2 and 3) such as wing fences, engine location, V-Tails, translating L.E. and T.E. controls (reducing sweep with increasing deflection) etc.

Revival of the interest in FSW is due to the work of Krone (Refs. 4-8). He indicated that the main problem of aero-elastic divergence for higher forward sweep can be overcome with an aero-elastically tailored wing using composites. Such a wing is stiff in torsion and does not have undue weight penalties. This discovery coupled with the advances in related technology eg. incorporation of favourable aerodynamic interferences, active control and propulsion emphasised re-consideration of FSW for several aircraft types. The Defence Advanced Research Projects Agency (DARPA) in USA initiated Studies and a design competition in 1976 for a FSW combat aircraft manned demonstrator with three contractors - General Dynamics, Grumman and Rockwell. The winner, Grumman X-29 (Fig. 3), is now undergoing flight trials. This aircraft is designed with a low aspect-ratio canard and an aspect-ratio 4 FSW (L.E. at -30°). It uses a F-5 forebody and components from other current aircraft. Several papers (Refs. 9-14) have been recently devoted to the detail on the X-29 and its work progress.

In 1980, Truckenbrodt (Ref. 15) presented a case for high aspect ratio FSW designs. The constraints in his study on FSW and ASW with mid-chord sweep of 45° (Fig. 4) were two fold: (i) that optimised twist is present to ensure elliptic spanwise load distribution at cruise C_L = 0.45 and (ii) that the onset of flow separation is inboard at C_L = 1.0. He showed that a FSW of aspect-ratio 9 compares with an ASW of aspect-ratio 12.5 in satisfying constraint (i) but the constraint (ii) is satisfied by the FSW only thus indicating its superiority.

The resurgence of interest in FSW's led to an International Conference at Bristol in 1982 (Ref. 16) at which some 31 papers were tabled. Research and Development (R & D) studies on several aircraft types with low and high aspect-ratio FSW's were presented. The R & D and configurational work has been sustained with somewhat increased momentum in USA.

Figs. 5-9 depict some of the current ideas with regard to high aspect-ratio wings. Such aircraft are expected to exploit the known advantages of the FSW eg. lower lift induced and profile drag, appreciable natural laminar flow (Refs. 17-19) near the wing tips and better performance at high C_L. Some designs feature the low interference mid-or high-wing locations.

Fig. 5 depicts the Learjet LRXX proposal for an "Executive" Canard-FSW design for the year 2000 AD. This has Mach 1.8 capability (Ref. 20). However, on a smaller time-scale Cook and Abla (Ref. 21) refer to a study on adapting a FSW on the Learjet model 55 (Fig. 6) by reversing the 20° L.E. sweep. A Beechcraft FSW high-tail supersonic design (Ref. 22) is shown in Fig. 7.

Roskam (Ref. 23) has proposed a 3-surface "commuter" aircraft (Fig. 8). Such a configuration offers the possibility of optimum arrangement of major components including undercarriage. Trim drag can be minimised at all flight altitudes. A canard-FSW commuter (Fig. 9) has been shown by Rutan (Ref. 24).

The high-wing designs are characterised by the Lockheed Canard-FSW concept as shown in Fig. 10. Smith and Srokowski (Ref. 25) have compared an ASW and several "equivalent" cranked FSW planforms. They indicate that a FSW with a cranked T.E. can be designed without any transonic penalties. Canard is favourable.

Nangia (Ref. 26) has presented some theoretical comparisons for high aspect ratio transport FSW & ASW. He has also discussed several 'pros and cons' for the FSW arrangements.

This paper relates to subsonic longitudinal test and analysis conducted on two series of configurations with wings of aspect ratio near 8. The aims are to gain an understanding of the FSW technology in the high aspect ratio range, and to indicate areas for future work.

The first series represent "Transport" types (high-wing) and the second, "Executive" (Business-Jet) types. In each series of models, FSW and ASW could be incorporated with the sweep angle reversed about 25% chord. For the FSW this approach implies a reduction in L.E. sweep by

about 5°, and a increase in sweep by 10° at the 3/4 chord-line (approximate location of transonic shock). This approach yields therefore a 'faster transonic' FSW. There are other possible 'sweep equivalence' criteria eg. Shaw (Ref. 27) suggests 33% chord-line sweep and Weeks et al (Ref. 28) suggest 80% line.

II. MODELS & WIND TUNNEL TESTS

II.1 "Transport" Aircraft (TFSW & TASW)

A conventional transport aircraft features a high wing and a "butterfly-tail" set high on the fin clear of the wing wake throughout the whole operating α- range. The undercarriage is stowed away in the fuselage. High wing situation is favourable to FSW on 2 counts: (i) it allows an increase in dihedral stability, and (ii) The FSW requires wash-in twist, cruise lift and cabin floor requirement then imply that the wing root incidence on the body is near zero. This allows a smooth wing-body junction with the required transonic capability. With a conventional ASW and wash-out twist, cabin floor requirements imply a positive 3° to 5° wing setting angle on the body. The junction therefore requires careful design.

These considerations have led to design of configurations shown in Figs. 11 and 12 and geometry as given in Table 1. TFSW series denote the FSW models and TASW series the ASW models.

The TFSW tests were on 4 basic combinations:

F	FSW & Body (wing with wash-in twist)
CF	Canard (low) + FSW & Body
FT	FSW & Body + Tailplane (above the fin)
CFT	Canard (low) + FSW & Body + Tailplane (high) - 3 surface concept

The tests covered the effects of wing root fillets, winglets (tip-fins), L.E. and T.E. devices.

The TASW test combinations were:

A	ASW & Body (wing with wash-out twist)
AT	ASW & Body + Tailplane (above the fin)

The effect of winglets was also covered.

II.2 "Executive" Aircraft (EFSW & EASW)

As mentioned earlier, one of the main advantages of using FSW in an "Executive" type is that the wing root (near zero incidence) can be located behind the cabin in a mid-wing location. With an ASW, the wing root area (with a positive incidence) has to be set under the cabin which in turn requires an extensive fillet. Table 2, Figs. 13 and 14 refer to geometry and details of the "Executive" type aircraft with alternative wings: the mid-wing FSW (EFSW series) and the low-wing ASW (EASW series). The design of the models had the benefit of incorporating certain ideas and knowledge gained from the previous studies on the "Transport" types. Notable among these ideas was the use of a cambered aerofoil section NACA 241X series (X=0 at tip, = 5 at root) to help achieve a higher C_{Lmax} at low Reynolds number.

The EFSW tests were on 4 basic combinations (as for TFSW):

F	FSW (mid-wing) & Body (wing with wash-in twist)
CF	Canard (low, with and without anhedral) + FSW & Body
FT	FSW & Body + Tailplane (above the fin)
CFT	Canard (low) + FSW & Body + Tailplane (high) - 3 surface concept.

The tests covered the effects of winglets, boundary layer fences, L.E., T.E. devices and nacelles.

The EASW tests on two combinations were:

A	ASW (low-wing) & Body (wing with wash-out twist)
AT	ASW & Body + Tailplane (above the fin)

The effect of winglets and nacelles were also covered. The nacelle location on the EASW is not identical to that on the EFSW. No attempts have been made at optimising the geometry of winglets or nacelle location.

II.3 Wind Tunnel Tests

Tests were conducted in the University of Bristol 3.5 ft Open Jet Wind Tunnel at a speed of 110 ft/sec. The wind tunnel is equipped with a manual overhead 3-component balance.

Each model was mounted conventionally (upside down) on the balance with struts and hinged pivots on the wing lower surface. A pitch-wire attached to a metal sting through rear of the fuselage, completed the rig-assembly.

Early preliminary tests with transition strips applied to the wing surfaces, indicated that the data obtained was unreliable and subsequent work was therefore carried out with transition strips applied to the fuselage nose only.

III. TRANSPORT TYPE AIRCRAFT (TFSW & TASW)

III.1 Theoretical Considerations - Lifting Surface Calculations

Lifting surface calculations using method of Ref. 29 have been undertaken to provide a feel for the magnitude of interference between various surfaces. These calculations also indicated the likely locations y_L (stall onset from the peaks in spanwise local lift C_{LL} distribution) and y_{cp} (spanwise centre of the half-wing load).

For simplicity, the lifting surfaces are considered to be thin; the wakes are assumed planar and they lie parallel to the body-axis. This technique avoids any wake intersections. Fuselage effects have not been included.

Fig. 15 shows the C_{LL} distributions for the FSW and ASW configurations (zero wing twist). These confirm that the FSW is less prone to wing-tip stall. A canard is effective in reducing the wing root loading.

Fig. 16 and 17 show the effect of wing twist (+5° wash-in on the FSW and -5° wash-out on the ASW). At low α, the effect on FSW is particularly marked; y_L moves nearer to the wing tip. With increasing α, y_L moves inboard. For the ASW the effect of twist at low α is to move y_L inboard and at higher α, to move it outwards toward the tip and near to the plane ASW location. y_{cp} displays similar trends; the movements are smaller because this is an integrated effect.

Fig. 18 shows the canard effect on the FSW with +5° wash-in twist; the tendency (cf. wing alone Fig. 16) is to move y_L slightly inboard.

Fig. 19 summarises the positions y_L and y_{cp} on various combinations of TFSW and TASW. y_L is near zero for the planar FSW and about 3/4 span for the planar ASW. The canard effect on FSW is to move y_L and y_{cp} both outwards.

III.2 Experiments on TFSW Series

III.2.1 F, CF, FT, CFT Combinations

Fig. 20 illustrates the lift, drag and pitching moment relationships. The canard and the tailplane are both set at 0° incidence. The results are not trimmed and are based on gross wing area. The basic wing-body configuration (F) shows the onset of non-linearity and hence flow separation at C_L above 0.52. This is accompanied by pitch-up tendency. This is not entirely surprising in view of the uncambered NACA 0015 wing aerofoil section. This configuration shows a gentle stall at about 11° angle of attack (C_L = 0.71) followed by regaining of lift beyond α = 14° to C_L = 0.86 at α = 25°.

Addition of canard (CF configuration) leads to increase in C_L, a forward shift of neutral point, softer stall and pitch-up. This suggests that the canard aids in relieving the FSW root separation problem. Flow visualisation studies suggested that the tip vortices from the low canard tend to trail over the wing upper surface through most of +α range. The C_m-C_L curve does not indicate any sharp 'breaks' to correspond with 'crossing' of the canard wake over the wing L.E.

The FT configuration C_L curve essentially follows the wing-body (F) curve with the inclusion of the contribution due to the tailplane in wing downwash flowfield. Similarly the CFT curve follows the CF curve. The tailplane in the CFT configuration is subject to the downwash fields of the canard and the wing both.

It is interesting to note that even though the exposed area of the canard is only 61% of the tailplane area, the additional lift due to the canard (CF configuration) and the tailplane (FT configuration) become equivalent at α = 17°. This effect is primarily because canard senses the upwash of the wing and the tailplane the downwash due to the wing.

From the L/D viewpoint and due to small scale Reynolds No., it is appropriate to look at C_L's upto about 0.6, prior to the onset of flow separation and non-linearities. The following table assists in evaluating peak L/D and approximate C_L at which the peak occurs.

Configuration	C_L	Peak L/D	L/D
F	.57	16.3	0
CF	.57	15.9	- 2.4%
FT	.57	16.1	- 1.2%
CFT	.57	15.0	- 9.2%

The peak L/D for the 3-surface CFT configuration is the least and accounts for the lack of trim and additional surface interferences present. This preliminary look suggests more detailed calculations of trimmed L/D with equivalent trimming volume ratios, as well as examination of optimised trimming surface areas. The relative sizes of the canard and the tailplane may be varied to obtain correct stall behaviour.

Location of Neutral Points

C_{mo} and neutral point positions for various combinations are shown in the following table. Component effects due to the canard and the tailplane have also been identified.

	F	CF	FT	CFT
C_{mo}	0	-.05	+.145	+.030
x_{ac}	.163$\bar{c}$	-.143$\bar{c}$	.517$\bar{c}$	.147$\bar{c}$

Component	Canard	tail	Canard + tail
ΔC_{mo}	-.050	+.145	+.030
Δx_{ac}	-.306$\bar{c}$	+.354$\bar{c}$	-.016$\bar{c}$

The C_{mo} effects are mainly a function of the fuselage shape and the control surface deflection with respect to the wing incidence on the body. The neutral point shifts forward with the canard and aft with the tailplane. The tailplane 'shift' is slightly higher due to its larger exposed area.

III.2.2. The Effect of Canard Deflection

Fig. 21 shows the effect of Canard deflection δ_c = -5°,0°,+5°. It is noted that:

(a) Increasing δ_c leads to increase in lift at lower α but at higher α the canard stall approaches earlier and there is an evidence of pitch-down.

(b) The control power in pitch due to the canard is nearly constant upto C_L = 0.6; thereafter it decreases.

(c) Positive δ_c leads to a loss in L/D. Negative δ_c improves L/D between C_L range of 0.5 to 0.7.

The estimation of trimmed results is dependant on actual C_{mo} of the configuration which in turn is dependant on several features eg. fuselage nose, interference effects, nacelles.

III.2.3 The Effect of Winglets (Fig. 22)

The winglets in this configuration have an effective L.E. sweepback of 43° + 5° (due to wing twist) = 48°. The main effects are:

(a) Increased loading near the tip leads to higher lift slope. The stall is relatively 'sharper'.

(b) L/D increases for C_L's above 0.28. Peak L/D value improves from 16 to 17.6 (10%).

(c) The neutral point is relatively unaltered, but the C_{mo} changes from -.045 to -.055.

III.2.4 Tailplane Deflection

FT & CFT Configurations are considered:

FT Configuration

Fig. 23 indicates that + δ_T leads to positive increment in C_L and a negative C_{mo}. The position of the neutral point is relatively unaltered at low C_L's. At C_L about 0.5 there is a tendency for pitch-down. At high C_L's, there is evidence of tailplane stall as the lift increment due to the tail reduces for α beyond 12.5°. The tailplane control power in pitch is twice that of the canard and this corresponds to the estimates of the relative trimming volume ratios.

CFT Configuration (Fig. 24)

The - δ_T curve shows a tendency for pitch down at higher C_L's whilst the + δ_T curve suggests the opposite. Comparison with Fig. 23 (FT configuration) indicates that the presence of canard reduces the tailplane control power in pitch. This is due to higher total downwash present at the tail in the CFT configuration. With reference to Fig. 21 (CF configuration), an assessment of combinations of δ_T and δ_c for trimmed flight can be made:-

δ_c	0°	+0.8°	+1.6°
δ_T	-2°	0°	+2.0°

It is obvious that several combinations are possible. The idea here is to optimise L/D without any adverse effect on the flow at the wing root. At low C_L's, a small δ_c may provide a better L/D. At higher C_L's the wing root may be protected with larger canard positive δ_c and hence this will be accompanied by larger + δ_T.

III.2.5 L.E. & T.E. Devices on CF

Ref. 30 shows that a L.E. device (eg. a drooped flap or slat) located in the mid-semi-span region is very effective in delaying the wing root flow separation on a FSW. In view of the low Reynolds number induced flow separations present on this model, it was decided to try an "ad-hoc" approach with a simple "extended" thin flap attached at the L.E. No attempt was made at optimising either the deflection angle or the planform shape. The effect of the L.E. device is illustrated in Fig. 25. $C_{L_{max}}$ improves from 0.76 (α = 10°) to 1.11 (α = 25°). This improvement is accompanied by pitch-down at C_L = 0.85, whereas the basic configuration has a pitch-up tendency at C_L near 0.6. The L.E. device with its particular geometry implies a drag increase upto C_L = 0.7, thereafter there is marked reduction in drag and a corresponding marked increase in L/D.

A simple "extended" T.E. flap (one deflection angle) in combination with the L.E. device was used to give an idea of the high lift potential. An improvement in $C_{L_{max}}$ by about 0.43 to 1.48 was noted. An increase in lift curve slope was also obtained; this is due to an increase in effective lifting surface area. The L/D curve is extended beyond C_L = 0.85.

It can be inferred that there is a considerable scope for optimisation of T.E. devices in combination with L.E. devices of various types.

III.3 Experiments on TASW Series

III.3.1 Tailplane Effect

Fig. 26 shows the effect of a tailplane and its deflection on the wing body. Lift and pitching moment 'breaks' from linearity occur near C_L = 0.7. Maximum lift occurs near α = 7.5° and this is followed by a sharp stall.

Peak L/D of 16.2 for the wing-body occurs at C_L = 0.62. With the addition of tailplane, the peak L/D becomes dependent on δ_T and occurs at higher C_L values.

III.3.2 Effect of Winglets

This effect has been investigated for two configurations: Wing-body (A) and with tailplane (AT). The results in Figs. 27 and 28 show that at low C_L's the winglets produce a penalty in L/D. At higher α's, a small improvement in lift leads to about 3% improvement in L/D. For α's beyond stall, the effect due to winglets is minimal.

III.4 Comparison of TFSW (CF) and TASW (AT)

In these comparisons, the winglets play an important role. Fig. 29 shows the effect on L/D. The FSW configurations offer substantial gains for C_L above 0.3, whilst the ASW configuration shows small gains beyond C_L = 0.73. The effective L.E. sweepback of the winglets on the FSW is higher by 10°.

Fig. 30 shows the longitudinal relationships. One AT configuration is shown. The CF configuration includes two variations - F1 with and F2 without wing root fillets. The root fillets lead to slight increase in lift but penalise the peak L/D. As indicated earlier the Reynolds number and flow separation effects become increasingly dominant above C_L = 0.7. Nevertheless important conclusions can be drawn:-

(a) The AT configuration has slightly higher lift curve slope. Compared with the F1 and F2 configurations. The Reynolds number effects are possibly less severe with regard to stall onset on the AT configuration. Flow separations on the AT appear at wing tips where the chord is smaller than at the wing root. Flow separation generally begins in the wing root area on the FSW. The non-linearity on the AT curve begins at about C_L of 0.8; On the FSW it is nearer C_L of 0.65.

(b) With a mid-semi-span L.E. flap the onset of non-linearity of the Fl curve can be delayed to C_L of above 0.8. Thereafter the behaviour is extremely gentle and C_L of 1.1 is attained. It must be emphasised, that the flap geometry is not optimised.

(c) Peak L/D values are analysed with the aid of the following table:-

		Basic	Basic + Winglets
AT	C_L	.68	.69
	L/D (Peak)	15.1	15.1
	Ratio	1	1
CF	C_L	.58	.62 (Estimate)
	L/D (Peak)	16.8	18.4 "
	Ratio	1.113	1.218 "
CF Wing Root Fillets	C_L	.58	.62
	L/D (Peak)	15.9	17.5
	Ratio	1.052	1.159

The basic CF configuration without wing root fillets offers about 11% better L/D over the AT configuration. The winglets on the CF configuration lead to an extra 10% bringing the total improvement to 21%. The wing root fillets on the CF configuration appear to give a penalty of 5% in L/D as shown. This indicates that an accurate and optimised design of wing root junction is mandatory.

IV. EXECUTIVE TYPE AIRCRAFT (EFSW & EASW)

IV.1 Theoretical Considerations - Lifting Surface Calculations

The principle of these calculations is similar to that for the "Transport" type (III.1).

Fig. 31 shows the C_{LL} distributions at various α for the trimming surfaces (canard or tailplane). The effect of 10° anhedral is also depicted. The aft swept surface emphasises the loading near the tip (peak (y_L) at 80% semi-span); anhedral has an insignificant effect.

Fig. 32 shows the effect of +3° wing twist on the C_{LL} distributions. For the planar FSW, y_L is near the centre-line. Presence of twist leads to y_L movement to near the wing tip at low α, but at higher α, y_L moves inboard as the comparative effect of wing twist decreases.

Figs. 33, 34 and 35 show the effect of canard (with and without 10° anhedral) on the planar and twisted FSW's. The essential effects are reduction of root loading on FSW and increase of loading on the canard. Canard anhedral implies a small relief in interference because the canard tip is further away from the wing.

Fig. 36 summarises the positions y_L and y_{cp} on various CF combinations (canard anhedral and wing twist). These support the inferences from the previous Figs. 32-35.

Figs. 37 and 38 show the local lift distributions on the planar and -3° twisted ASW's. The positions of peak lift (y_L) and the centre of spanwise load are given in Fig. 39. The aft swept wing produces heavier loading near the tip, the effect of twist is to move both y_L and y_{cp} toward the centre at low α, but at higher α, both tend to move near the tip.

IV.2 Experiments on EFSW Series

IV.2.1 F, CF, FT & CFT Combinations

Fig. 40 illustrates the lift, drag, pitching moment relationships. The canard and the tailplane are both set at 0° incidence. The results are not trimmed and are based on gross wing area. The basic wing-body configuration (F) shows the onset of non-linearity and hence flow separation, and increase in C_D at C_L above about 0.65. This is accompanied by pitch-up tendency; C_L however continues to increase throughout the α range.

Addition of the canard (CF) leads to an increase in C_L, forward shift of neutral point and a gentler 'pitch-up'. This suggests that canard aids in relieving the FSW root separation problem.

The FT configuration C_L curve essentially follows the wing-body (F) curve with the inclusion of the contribution due to the tailplane in wing downwash flowfield. The neutral point moves aft.

The CFT configuration C_L curve follows the CF curve. The tailplane in the CFT configurations is subject to the downwash flowfields of the canard and the wing both. Thus incremental lift coefficient (ΔC_L) due to canard and tail together as measured is slightly less than the sum of the individual ΔC_L's of the canard and tailplane.

It is interesting to note that even though the exposed area of the canard is only 52% of the tailplane area, the lift gain due to the canard is greater at α's above 15°.

From the L/D view point and small scale Reynolds No., it is appropriate to look at C_L's upto about 0.7, prior to the onset of flow separation and non-linearities. The following table assists in evaluating peak L/D and C_L's at which the peaks occur:-

Configuration	C_L	Peak L/D	L/D
F	.52	20.0	0
CF	.56	18.2	- 9.9%
FT	.63	18.4	- 8.0%
CFT	.58	17.0	-15.0%

The canard and the tailplane, when used individually, cause 8 - 10% reduction in L/D, but in combination together they cause only a 15% reduction. This preliminary look suggests more detailed calculations of trimmed L/D with equivalent trimming volume ratios as well as examination of optimised trimming surface areas. The relative sizes of the canard and tailplane need to be varied.

Location of Neutral Points

C_{mo} and neutral point positions for various combinations are shown in the following table. Component effects due to the canard and tailplane have also been identified.

	CONFIGURATION			
	F	CF	FT	CFT
C_{mo}	- .015	- .093	.220	.155
x_{ac}	.208$\bar{c}$	- .320$\bar{c}$	.856$\bar{c}$	.281$\bar{c}$
component	Canard	tail	Canard + tail	
ΔC_{mo}	- .078	+.235	+.170	
Δx_{ac}	- .527$\bar{c}$	.648$\bar{c}$	+.073$\bar{c}$	

The C_{mo} effects are mainly a function of fuselage shape and control surface deflection with respect to the wing incidence on the body. The neutral point shifts forward with the canard and aft with the tailplane. The tailplane 'shift' is higher due to the larger effective exposed area.

IV.2.2 The Effect of Wing Root Incidence i_w on the Body

This effect has been derived from tests with and without the canard. These tests aid in obtaining a reasonable configuration with positive wing lift at zero body/cabin floor attitude.

Wing-Body only (F) (Fig. 41)

It is inferred that:-

(a) As i_w increases so does C_L at $\alpha \approx 0$.

(b) Comparison with the 2-D $C_L - \alpha$ curves for NACA 2412 section (experiments at R = 0.4 x 10^6, theoretical results extrapolated to R = 0.4 x 10^6 from Ref. 31) indicate that lift on the wing-body combination is subject not only to the aspect ratio effect but also to possible non-linearities in the flow above C_L = 0.7. There is no apparent sharp stall behaviour. This reflects one of the important features of the FSW - the stall on the wing begins near the wing root.

(c) Increase in i_w leads to negative pitching moment C_{mo} at zero C_L. This tendency is primarily due to the fuselage attitude being negative at zero lift of the wing.

(d) The position of neutral point at low C_L is relatively unaffected by i_w. The pitch-up tendency becomes worse as i_w increases.

(e) L/D reduces slightly as i_w increases. This is possibly due to larger interference between the wing and the body.

Wing & body and canard (CF) (Fig. 42)

The canard is set at zero angle of attack.

(a) The $C_L - \alpha$ curves show increase in lift due to the canard. The canard also has increased interference lift due to the wing. This interference lift increases as α increases.

(b) The L/D - C_L characteristics show that i_w effect is small. To some extent the effect is being masked by the fact that the canard is set at -5° incidence relative to the wing root incidence.

(c) Increase in i_w leads to a negative pitching moment C_{mo}. This appears to be large only because the canard is set at -5° incidence with respect to the wing root.

(d) The neutral point of the configuration at low C_L is relatively unaffected by i_w. The pitch-up tendency arises at lower C_L as i_w increases.

IV.2.3 The Effect of Canard Deflection

Fig. 43 shows the effect for 3 settings of δ_c = -5°, 0° and +5°. It is noted that:

(a) As δ_c increases, the canard 'stall' approaches at earlier C_L.

(b) The pitch control power of the canard with + δ_c reduces with increasing C_L. On the other hand, - δ_c pitch power remains constant up to C_L = 0.8.

(c) As may be anticipated, placing a canard on a wing-body combination implies a penalty on L/D. This is true for C_L's below about 0.7. At higher C_L's however, due to increase in canard lift, this L/D penalty disappears and there is a net gain. $-\delta_c$ improves L/D for C_L's between 0.6 and 0.8.

IV.2.4 Effect of Canard Anhedral

Canard anhedral implies two basic effects on lifting characteristics, (i) to reduce the canard lift and (ii) to re-position the canard wake in relation to the wing thus reducing the canard induced interference on the wing at low α. At high α, the canard tip vortices approach the wing leading edges.

Fig. 44 shows that at α = 19°, the overall lift on the configuration reduces with canard anhedral. Thereafter there is a slight increase in lift; this however is not a fully established trend. Further work is required.

IV.2.5 Effect of Wing Fences

The fences were located at η =0.35 downstream of the maximum aerofoil thickness point (physical dimensions: length 2.6 in., height at start .15 in., height at wing T.E. = 0.5 in., maximum width = .06 in. The effect of wing fences has been examined for two configurations first for the basic wing body (F) and then with a canard (CF) (Figs. 45 and 46). Percentage improvement in L/D for both configurations is shown in Fig. 47.

For the wing body (F), the beneficial effect of the fences is apparent at C_L's above 0.29. The fences delay the flow separation by reducing the spanwise inwards drift of the boundary layer flow. L/D improvements of the order of 7% in the C_L range from .35 to .6 are obtained. At large values of C_L's, the fences become submerged in the flow and their effectiveness decreases. The wing fences produce a small $-C_{mo}$ at zero C_L. The pitch-up tendency is delayed and a slightly higher C_L is obtained with fences.

For the wing + body + canard (CF) combination, the fences produce higher lift and $-C_{mo}$ as illustrated. The beneficial effect of the fences is particularly apparent above C_L = 0.5. L/D improvements of the order of 4% at C_L = 0.6 and 8% at C_L=0.7 are obtained. It is deduced that at lower C_L's, the effect of fence is minimal because the canard induced velocity distribution tends to reduce the inward spanwise drift of the boundary layer on the wing in any case, and the fences are then in straightened flow already. At higher C_L's, delaying the flow separation implies large gains in L/D.

IV.2.6 The Effect of Winglets (Fig. 48)

The winglets in this configuration have an effective L.E. sweepback of 53° + 3° (due to wing twist) + 5° (due to i_w) = 61°. The effects are:-

(a) Increased loading near the tip leads to higher lift curve slope.

(b) L/D increases at C_L's above 0.25. Peak L/D improves from 18 to 19.3 (7.2%).

(c) The neutral point moves aft (3% c) with a slight increase in $-C_{mo}$ (from -.2 to -.22 ie. 10%).

By reducing the L.E. sweepback of the winglet (c.f. TFSW), higher L/D gains may be produced. This will be considered in IV.4.

IV.2.7 Tailplane Deflection on FT

Fig. 49 illustrates the basic effects due to tailplane deflection. Curves for the wing body are also presented.

Positive deflection δ_T of the tailplane leads to positive imcrement in C_L and negative pitching moment C_{mo} at zero lift. The position of the neutral point is relatively unaltered at low values of C_L. At high C_L for $+\delta_T$, there is evidence of tailplane stall as lift increment due to the tail reduces beyond α = 12.5°.

The tailplane control power in pitch is about 1.5 times larger than the canard control power. This is approximately in line with the estimated trimming volume ratios.

IV.2.8 Effect of Nacelles

The effect of adding nacelles has been examined for two configurations F and FT in Figs. 50 & 51. The main effects are:-

(a) ΔC_L = about 0.05 at C_L = 0 which progressively decreases and vanishes at about α = 12.5°.

(b) Pitching moment - For the wing-body (F) combination, the nacelles provide + C_{mo} but at higher C_L, the pitching moment is negative. The FT configuration produces a constant -ve contribution in C_m.

(c) L/D curves show an increase in drag due to the nacelles.

Nacelle location has not been optimised and work with regard to quality of intake flow is required.

IV.2.9 CFT Configuration

Fig. 52 shows the longitudinal relationships for a few values of tailplane and canard deflections. Wing-body only curve is also illustrated. All the curves are nearly straight horizontal lines parallel to the C_L axis upto C_L = 0.7. This implies that the hinge point of the model coincides with the neutral point of the CFT configuration. The canard control power is roughly half that of the tailplane. This is approximately in line with the trimming volume ratios. This enables an assessment to be made of δ_c and δ_T required for trimmed flight as follows:-

δ_T	δ_c	
0°	-5°	lower C_L's
+2°	0°	
+4.5°	+5°	higher C_L's
+5°	+6°	

Obviously many combinations are possible. The idea here is to optimise L/D without having an adverse effect on the root flow over the wing. At cruise type C_L's therefore a negative or small δ_c may provide a better L/D. At higher C_L's however the canard effect on the wing root may need to be increased and so δ_c will be positive and this will be accompanied by a positive δ_T.

IV.2.10 L.E. & T.E. Devices on CF

As for the TFSW-CF Configuration it was decided to try an 'ad-hoc' approach to delay the onset of flow separations with a simple L.E. flap. No attempt was made to optimise the deflection angle or the planform shape of this flap. The effect of the device is shown in Fig. 53. The effect on the C_L and C_m characteristics is particularly significant and the linear part of the curve is maintained to about C_L = 1.1. As might be expected, the flap incurs a drag penalty for C_L's below 0.8. At higher C_L's however L/D is improved.

A simple "extended" T.E. flap (one deflection angle) in combination with L.E. flap was used to give an idea of the high lift potential. An improvement in C_{Lmax} by about 0.53 to 1.62 was noted. An increase in lift curve slope was also obtained; this is partly due to increase in the effective lifting surface area. The L/D curve is extended beyond C_L = 0.92.

It can be inferred that there are possibilities for optimising the T.E. flap geometry in combination with L.E. devices of various types.

IV.3 Experiments on EASW Series

IV.3.1 Effect of Tailplane

Fig. 54 shows the effect of a tailplane and its deflection on the wing-body. Lift and pitching moment 'breaks' from linearity occur approximately C_L = 0.75. Maximum lift occurs at about α = 16° and this is followed by a sharp stall.

Peak L/D of 17.5 for the wing body occurs at C_L = 0.57. With the tailplane on, the peak L/D is dependant on its deflection but it occurs near C_L = 0.62.

IV.3.2. Effect of Winglets

This effect has been investigated for two configurations; wing-body (A) and wing-body + tailplane (AT). The results are shown in Figs.55 and 56. At low C_L the winglets produce a penalty in L/D. At higher angles of attack, a small improvement in lift leads to about 3% improvement in L/D. The angle of attack for occurrence of stall is earlier with the winglets on. For high C_L there is penalty in L/D again as winglets may encourage tip stall.

IV.3.3 Effect of Nacelles

The effect of adding nacelles has been examined for two configurations A and AT in Figs. 57 and 58. The main effects are:-

(a) Increase of lift-curve-slope and C_{Lmax}.

(b) Slight aft movement of neutral point at low C_L and pitch-down moment. This is more evident from the wing-body configuration only, as the tail partly overlaps the nacelles in plan-view.

(c) Reduction in L/D throughout the C_L range.

As remarked earlier, the nacelles are not located in any particular optimum position and further work on this topic will be required before any comparisons with the FSW configuration can be justified.

IV.4 Comparisons of EFSW (CF) and EASW (AT)

The winglets play an important role in these comparisons. Fig. 59 shows the effect on L/D. The FSW configuration offers substantial gains beyond C_L = 0.25, whilst the ASW configuration offers gains beyond C_L = 0.5. The effective L.E. sweepback on the FSW is higher by about 11°.

Fig. 60 is an attempt to correlate improvement in L/D at various C_L values against winglet L.E. sweepback for the FSW and ASW configurations of this paper. Reduction of winglet L.E. sweepback is beneficial.

Fig. 61 shows the longitudinal relationships. One AT configuration is shown. The CF configuration depicts variation of wing root incidence setting on the body (F1 is set at 0° and F2 at +5°). F1 produces slightly higher peak L/D (by 2.8%) than F2. F2 produces larger lift at α = 0°. As indicated earlier, the Reynolds No. and flow separation effects become increasingly dominant above C_L = 0.7, nevertheless some important conclusions can be drawn:-

(a) Compared with the F1 and F2 configurations, the AT configuration has a higher C_{Lmax} and a higher lift curve slope. The Reynolds number effects are possibly less severe on the AT than on the F1 & F2 configurations. The onset of non-linearity on AT is nearer C_L = 0.9 but the stall is sharper.

(b) With a mid-semi-span L.E. flap, the non-linearity of the F2 model can be delayed to about C_L = 1.1. Thereafter the behaviour is extremely gentle and C_L = 1.25 is attained. Further increases with an optimised flap are feasible.

(c) Analysis of the peak L/D values may be facilitated with reference to Table 3.

The basic CF configuration offers about 11% better L/D over AT configuration. Winglets on the F1 improve this figure to about 15%. A further improvement with optimised winglets might well lead to another 5-10% increase. The root stall on the FSW can be suppressed by incorporation of wing fences and upto 19% improvement in L/D can be obtained.

The inferences for L/D may be supported by looking at $C_D - C_L^2$ relationships (Fig. 62). The FSW configurations produce smaller C_{Do} and also smaller slope and hence show lower lift induced drag. Winglets also reduce the slope. It must be mentioned that more accuracy is needed in any future work as the configurations are not symmetrical with respect to C_L = 0 axis.

V. CONCLUDING REMARKS & FUTURE WORK

The benefits of FSW, eg. lower lift induced drag, improved high angle of attack behaviour have been appreciated for some time. Because of the structural divergence problem, however, these could not be fully exploited. With recent advances in the fields of composite structures, flight dynamics and propulsion, the FSW technology has come to forefront again. This paper relates to subsonic longitudinal tests and analysis carried out on two series of configurations with forward- and aft-swept wings of high aspect ratio near 8 - the aim being to gain an understanding of the FSW technology in the high aspect ratio range.

The first series represented the high wing "Transport" types and the second, "Executive" types. In each series of models, Forward- and Aft-swept wings could be incorporated with the sweep angle reversed about the 1/4 chord. Canard and high tail could also be represented. The FSW "Executive" type featured a mid-wing location behind the passenger cabin. The comparable ASW "Executive" type had the wing set low under the cabin.

An idea of 3-surface layouts was also obtained. Tests included the effects of winglets, leading and trailing edge flaps and wing fences.

Subsonic theoretical analysis shows:

(a) The basic FSW is generally lightly loaded at the tip and requires less wing twist + ve sense (wash-in), to attain elliptic or minimum drag loadings.

(b) As small α, wing twist on FSW has a strong effect on moving the spanwise location of the peak loading towards the tip. For higher α, the peak loading moves nearer to root.

(c) The canard effect is beneficial in providing a relief of the wing root loading at higher α.

(d) Wing root bending moment is generally less for the FSW.

The experimental results show that in spite of low test Reynolds No. (0.2×10^6 based on wing chord), several important conclusions can be drawn:

(a) Gentler stall and improved high lift characteristics for the FSW. Wing root design is important. Because of wash-in type twist requirement, the FSW has a lower wing root setting angle on the fuselage and therefore the interference effects can be reduced.

(b) Lift induced drag was in general less for the FSW types.

(c) Peak L/D for the configurations occurred near C_L=0.6 (ie. in the "linear" range and before Reynolds number and flow separation effects dominate). Compared with the equivalent ASW + tail configurations, the FSW + canard configurations produced about 15-20% higher L/D (exact value depended on presence of winglets, wing fences etc.)

(d) Winglets appeared to be 3-4 times more effective in L/D and C_L terms on the FSW compared with the ASW. They also aid the dihedral stability of the FSW.

(e) Reynolds No. effects are more apparent on the FSW and flow separations at the root affect larger proportion of the wing area. L.E. flaps located mid-semi-span were effective in delaying the FSW root flow separation.

The tests have made a strong case for further work on FSW's at higher subsonic and transonic Reynolds No. Lateral stability tests have also been indicated. FSW optimisation can be attempted by several means eg. by exploiting the reduced wing root bending moment, using extensive natural laminar boundary layer and using 3-surface layouts.

ACKNOWLEDGEMENTS

The author has been fortunate to have had the opportunity of participating in the FSW research over the last few years. Amongst many people consulted on both sides of the Atlantic, the author wishes to thank Col. Dr. Norris Krone, Dr. Thomas Weeks, Mr Glenn Spacht, Mr Michael Robinson (USA), Mr David Shaw, Mr Clifford Bore and Prof. Lewis Crabtree, Mr Peter Allard (UK), for their helpful, stimulating, timely advice and suggestions on FSW R & D in general.

Part of the work mentioned was supported under SERC (UK) grant at University of Bristol in co-operation with BAe and RAE.

Thanks are due to Mrs Susan Drew for typing of the script, Mr Julian Partridge and Mr Rodney Powis (SAC Technical Publications Division) for organising the pictorial work. Lastly it should be mentioned that the opinions expressed by the author in this paper are his own.

REFERENCES

1. WOCKE, H. & DAVIS, L.W., "Sweptforward Wings for the HFB 320 Hansa". Aircraft Engineering pp 248-51 (Aug 1964).

2. NEPPERT, H., "Chronik der HFB 320 Hansa". HFB Internal Report.

3. NEPPERT, H. & SANDERSON, R., "Some Investigations concerning the effects of Gaps and Vortex Generators on Elevator Efficiency and of Landing Flap Sweep on Aerodynamic Characteristics". AGARD-CP-262.

4. KRONE, N.J. Jr., "Divergence Elimination with Advanced Composites". AIAA-75-1009 (1975).

5. AVIATION WEEK & SPACE TECHNOLOGY, "Forward Sweep". 26 June 1978 p19.

6. WARWICK, G., "Forward Sweep - Rockwell's New Broom". FLIGHT INTERNATIONAL 17 Nov. 1979 pp 1660-62.

7. KRONE, N.J. Jr., "Forward Swept Wing Flight Demonstrator". AIAA-80-3047 (1980).

8. KRONE, N.J. Jr., "Forward Swept Wing Flight Demonstrator". AIAA-80-1882 (1980).

9. SPACHT, G., "The Forward Swept Wing, A Unique Design Challenge". AIAA-80-1885.

10. GRAFTON, S.B., GILBERT, W.P., CROOM, M.A. & MURRI, D.G., "High-Angle-of-Attack Characteristics of a Forward-Swept Wing Fighter Configuration". AIAA-82-1322 (1982).

11. MOORE, M., & FREI, D., "X-29 Forward Swept Wing Aerodynamic Overview". AIAA-83-1834 (1983).

12. GRIFFIN, K.E., & JONAS, F.M., "Wake Characteristics and Interaction of the Canard/Wing Lifting Surface Configuration of the X-29 Forward-Swept Wing Flight Demonstrator". AIAA-83-1835 (1983).

13. MURRI, D.G., CROOM, M.A., & NGUYEN, L.T., "High Angle-of-Attack Flight Dynamics of a Forward-Swept Wing Fighter Configuration". AIAA-83-1837 (1983).

14. MORISSET, J., "Un avion re'volutionnaire: le X-29A de Grumman". Air et Cosmos No. 976, 19 Nov. 1983 pp 21-22.

15. TRUCKENBRODT, E., "How to Improve Performance of Transport Aircraft by Variation of Wing Aspect-Ratio and Twist". ICAS, Munich 1980, Paper 80-0.1.

16. NANGIA, R.K., Editor. Proceedings of International Conference on "Forward Swept Wing Aircraft" University of Bristol. UK, March 1982.

17. McCORMACK, G.M. & COOK, W.L., "A Study of Stall Phenomena on a 45° Swept Forward Wing". NACA TN 1797 (1949).

18. HIRSCHEL, E.H. & SACHER, P., "A Comparative Study of the Boundary Layer Development on FSW's". See Ref. 16.

19. PAISLEY, D.J. & POLL D.I.A., "Laminar Flow and Transition on Swept Wings". See Ref. 16.

20. GATES LEARJET CORP. Announcement NBAA Meeting 23 Sept. 1980.

21. COOK, E.L. & ABLA, M., "Weight Comparison of Divergence-Free Tailored Metal and Composite Forward Swept Wings for an Executive Aircraft". See Ref. 16.

22. AVIATION MAGAZINE INTERNATIONAL p.65 1.2.83.

23. ROSKAM, J., "Forward Swept Wings and Commuter Airplanes". See Ref. 16.

24. POPULAR MECHANICS. "Technology Update. It's all in that funny wing on the nose". April 1982 p.203.

25. SMITH P.R. & SROKOWSKI, A.J., "High Aspect Ratio Forward Sweep for Transport Aircraft". AIAA-Paper 83-1832 (1983).

26. NANGIA, R.K., Aspects of Forward Swept Wing Research at the University of Bristol". See Ref. 16.

27. SHAW, D.E., "Experimental Investigation into FSW's for a Light-Weight Combat Aircraft". See Ref. 16.

28. WEEKS, T.M., UHUAD, G.C. & LARGE, R., "A Wind Tunnel Investigation of the Aerodynamic Characteristics of Forward Swept Wings". AGARD CP-285 (1980).

29. PETRIE, J.A.H., "Development of an Efficient and Versatile Panel Method for Aerodynamic Problems". Leeds University Ph.D. Thesis 1979. Also User Grid for the SPARV Panel PROGRAM, BAe, Brough, Note YAD 3382, (1981).

30. McCORMACK, G.M. & COOK, W.L., "Effects of Several Leading-Edge Modifications on the Stalling Characteristics of a 45° Swept Forward Wing". NACA RMA9D29 NACA/TIB/2126 (1949).

31. SMITH, A.M.O., "Remarks on Fluid Mechanics of the Stall". AGARD LS.74., Aircraft Stalling and Buffeting, (1975).

TABLE 1 "TRANSPORT" MODEL TFSW & TASW SERIES

		Wing FSW & ASW		Canard or Tailplane
Gross aspect ratio	A	8		5.143
Gross area, in.^{2}	S	196		20.25
Exposed area, in.^{2}		181.6		14.0 (Canard)
Span, in.	b	28		9
Centre-line (root) chord, in.	c_r	5.0		2.5
Tip Chord, in.	c_t	2.0		1.0
Taper ratio		0.4		0.4
Geometric Mean Chord, in.	$\bar{c}$	3.5		1.75
Aerodynamic Mean Chord, in.	$\bar{\bar{c}}$	3.7143		-
		FSW	ASW	
Sweep angle L.E.		-22.5°	+28°	+29°
1/4 chord		-25°	+25°	+25°
3/4 chord		+30.5°	+20°	
Twist		+5° Wash-in	-5° Wash-out	0°
Dihedral angle		0°		0°
Aerofoil section		NACA 0015		NACA 0010
Mounting		High on Fuselage -		low on Fuselage (Canard) High on Fin (Tail)

Winglets (2) Mounted upwards at the wingtips.

Height	2.1 in.
Root Chord	2 in.
Tip Chord	0.75 in.
Leading Edge Sweep Measured at the tip Chord	43°

Aerofoil Shape - Thin flat surface with rounded L.E. and Sharp T.E.

Fin

Gross Height measured from Fuselage Centre Line,	5.8 in.
Root Chord	4.5 in.
Tip Chord	2.5 in.
Leading Edge Sweep	26°
Aerofoil Section	NACA 0010

Fuselage

Diameter	3 in.
Length	25 in.

Pitching Moment

Spanwise Locations of Pivots 8.3 in. from centre line

Chordwise locations 0.221 $\bar{c}$ = 0.108 $\bar{\bar{c}}$ (FSW)
0.590 $\bar{c}$ = 0.728 $\bar{\bar{c}}$ (ASW)

Wing Location

	FSW	ASW
Wing Apex to Fuselage Nose, in.	14	9
Wing Root incidence i_w	0°	+5°

Canard Location (incidence variable)

Canard Apex to Fuselage Nose	2 in.
Distance between aerodynamic centres of FSW and Canard	8.7 in.
Distance between aerodynamic centres of FSW and Tail	13.3 in.
Vertical separation to wing plane	2.8 in.

Tail Location (incidence variable)

Tailplane Apex to Fuselage Nose	24 in.
Distance between aerodynamic centres of ASW and Tail	13.3 in.
Vertical separation to wing plane	4.0 in.

L.E. Device (TFSW)

Span	3.9 in.
Gross Chord (normal to L.E.)	0.50 in.
Exposed Chord (normal to L.E.)	.40 in.
Thickness	.06 in.
Location - mid semi-span at the L.E.	
Deflection (Approximate)	35° down

T.E. Device (TFSW)

Span	5.93 in.
Gross Chord (normal to T.E.)	0.75 in.
Thickness	0.06 in.
Location - inner edge in line with inner edge of L.E. device.	
Deflection (Approximate)	40° down

TABLE 2 "EXECUTIVE" MODEL EFSW & EASW SERIES

		Wing FSW & ASW		Canard or Tailplane
Gross aspect ratio	A	8.75		3.898
Gross area, in.^{2}	S	179.2		21.53
Exposed area, in.^{2}		164.5		11.18 (Canard)
Span, in.	b	28		9.16
Centre-line (root) chord, in.	c_r	4.8		3.7
Tip Chord, in.	c_t	1.6		1.0
Taper ratio		1/3		0.37037
Geometric Mean Chord, in.	$\bar{c}$	3.2		2.35
Aerodynamic Mean Chord, in.	$\bar{\bar{c}}$	3.5		-
		FSW	ASW	
Sweep angle L.E.		-27.5°	+32°	+46°
1/4 chord		-30°	+30°	+40°
3/4 chord		+35°	+24.5°	
Twist		+3° Wash-in	-3° Wash-out	0°
Dihedral angle		0°		0°
Aerofoil section		NACA 2415 Centreline NACA 2410 Tip		NACA 0010
Mounting		High on Fuselage (FSW) Low on Fuselage (ASW)		low on Fuselage (Canard) High on Fin (Tail)

Winglets (2) Mounted upwards at the wingtips.

Height	2.0 in.
Root Chord	1.6 in.
Tip Chord	1.0 in.
Leading Edge Sweep Measured at the tip Chord	53°
Aerofoil Shape - Thin flat surface with rounded L.E. and Sharp T.E.	

Fin

Gross Height measured from Fuselage Centre Line,	6.1 in.
Root Chord (on body)	5.0 in.
Tip Chord	3.7 in.
Leading Edge Sweep	45°
Aerofoil Section	NACA 0010

Fuselage

Diameter	3.16 in.
Length	26.2 in.

Pitching Moment

Spanwise Locations of Pivots	7.9 in. from centre line
Chordwise locations 0.281 $\bar{c}$	= 0.094 $\bar{\bar{c}}$ (FSW)
0.453 $\bar{c}$	= 0.725 $\bar{\bar{c}}$ (ASW)

Wing Location

	FSW	ASW
Wing Apex to Fuselage Nose, in.	17	10.7
Wing Root incidence i_w	0°,+5°	+3°

Canard Location (incidence variable)

Canard Apex to Fuselage Nose	2.6 in.
Distance between aerodynamic centres of FSW and Canard	9.7 in.
Distance between aerodynamic centres of FSW and Tail	13.6 in.
Vertical separation to wing plane	1.4 in.

Tail Location (incidence variable)

Tailplane Apex to Fuselage Nose	26 in.
Distance between aerodynamic centres of ASW and Tail	13.4 in.
Vertical separation to wing plane	5.75 in.

L.E. Device (EFSW)

Span	3.5 in.
Gross Chord (normal to L.E.)	0.53 in.
Exposed Chord (normal to L.E.)	.40 in.
Thickness	.06 in.
Location - mid semi-span at the L.E.	
Deflection (Approximate)	45° down

T.E. Device (EFSW)

Span	6.3 in.
Gross Chord (normal to T.E.)	0.53 in.
Thickness	0.06 in.
Location - outer edge in line with outer edge of L.E. device.	
Deflection (Approximate)	45° down

Nacelles (2)

Length	6 in.) Different locations
Diameter	1.58 in.) on EFSW & EASW

TABLE 3 "EXECUTIVE" TYPE EFSW (CF) & EASW (AT) PEAK L/D COMPARISON

	AT			CF					
				$i_w = 0°$ (F1)			$i_w = +5°$ (F2)		
	C_L	L/D	Ratio	C_L	L/D	Ratio	C_L	L/D	Ratio
Basic	.65	16.3	1.0	.55	18.3	1.116	.56	17.7	1.086
Basic + Winglets	.65	16.3+	1.0	.57	19.3	1.149	.58	18.7*	1.113
Basic + Wing Fence		-		.60	18.5*	1.134	.61	17.9	1.098
Basic + Wing Fence + Winglets		-		.66	19.5*	1.196	.67	18.9	1.159

\+ Inadequate peak L/D definition - stall approaches wingtip.

* Estimated on basis of F2 - Wind Tunnel Test on F1 not conducted.

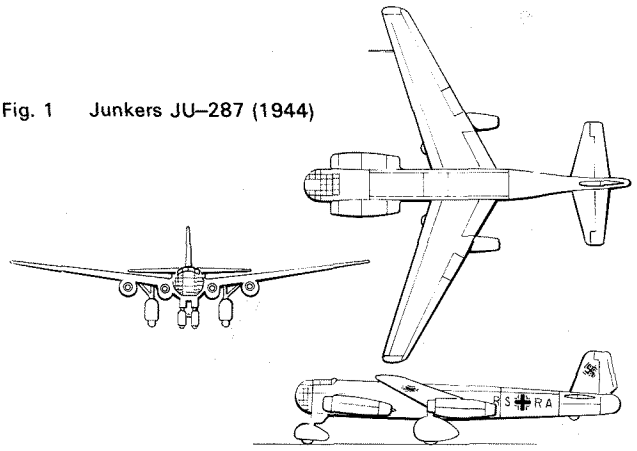

Fig. 1 Junkers JU–287 (1944)

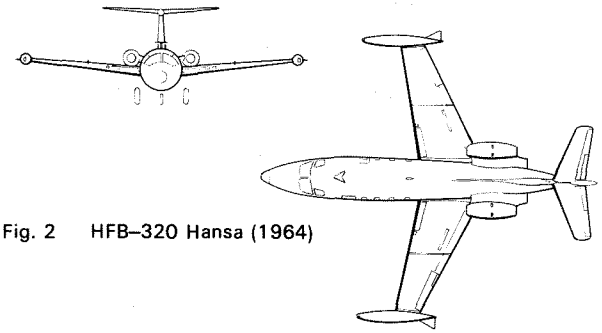

Fig. 2 HFB–320 Hansa (1964)

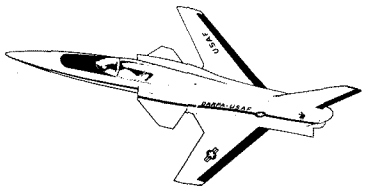

Fig. 3 Grumman X–29 (1984)

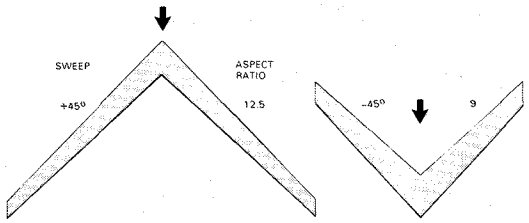

Fig. 4 Equivalent Performance ASW & FSW (Truckenbrodt)

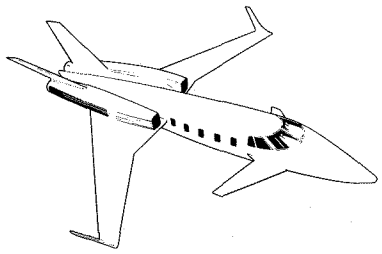

Fig. 5 Learjet Concept for 2000 AD (Canard + FSW)

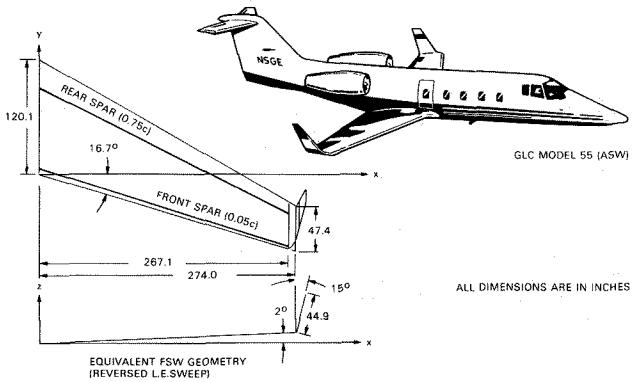

Fig. 6 Learjet Concept (Wing + Tail)

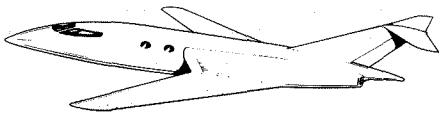

Fig. 7 Beechcraft Concept (FSW + Tail)

WING AREA	271 ft²
WING SPAN	57.4 ft
WING MGC	4.92 ft
WING ASPECT RATIO	12.1
CABIN WIDTH	107 in
CABIN AISLE HEIGHT	75 in
AIRPLANE HEIGHT	22.75 ft

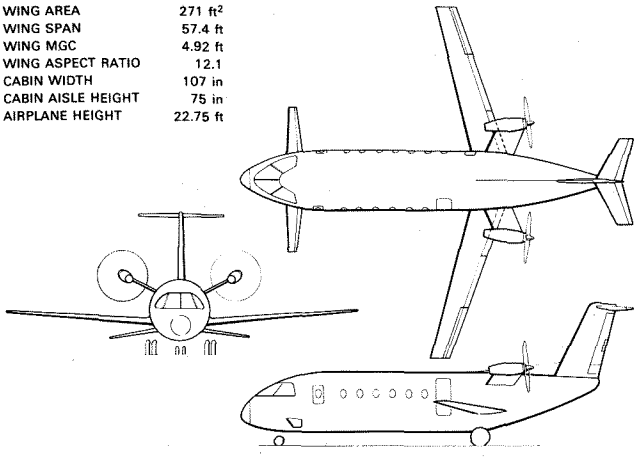

Fig. 8 3–Surface 30 Pax. FSW Configuration (Roskam)

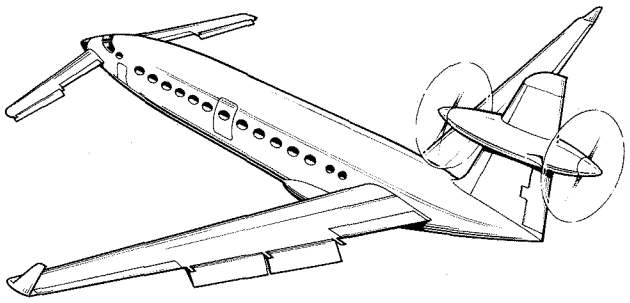

Fig. 9 36 Pax. Canard–FSW (Rutan)

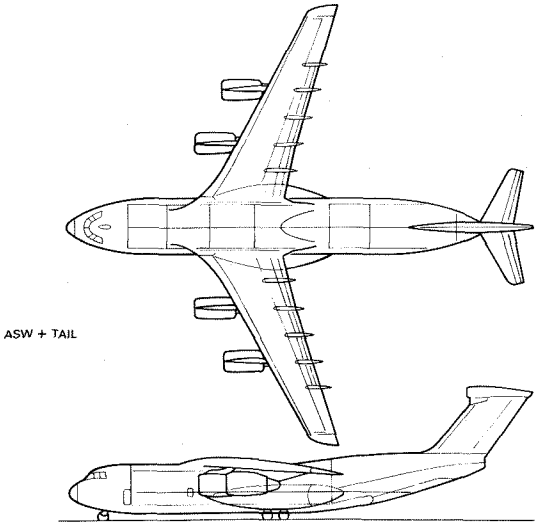

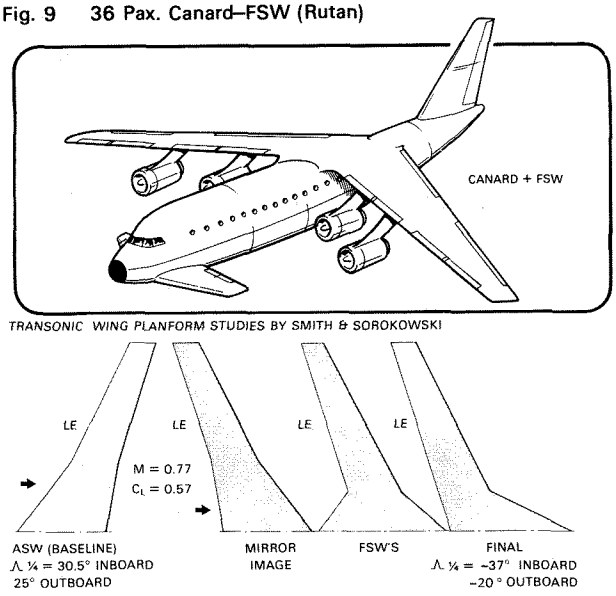

Fig. 10 Lockheed Transport Aircraft

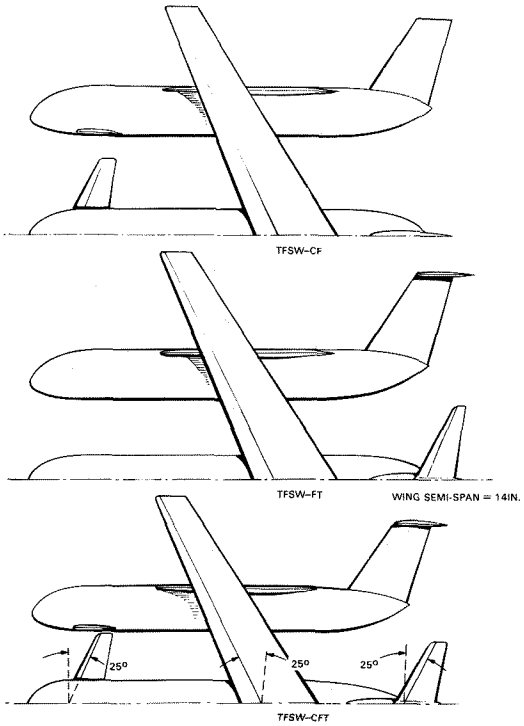

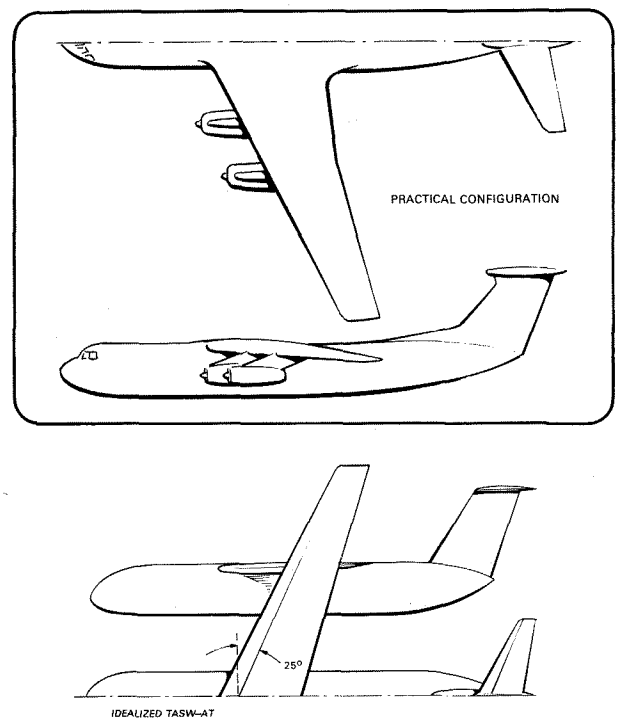

Fig. 11 "Transport" Type Aircraft Studies

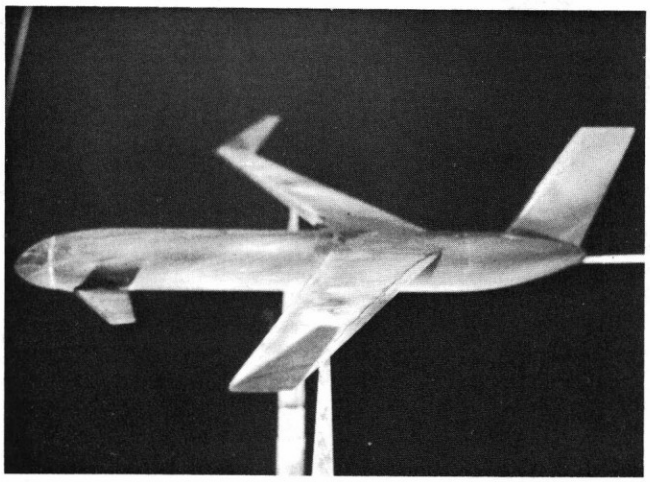

Fig. 12 TFSW–CF Wind Tunnel Model with Winglets

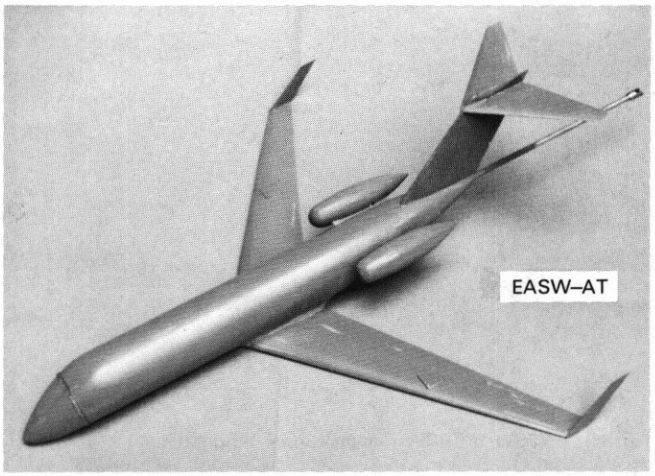

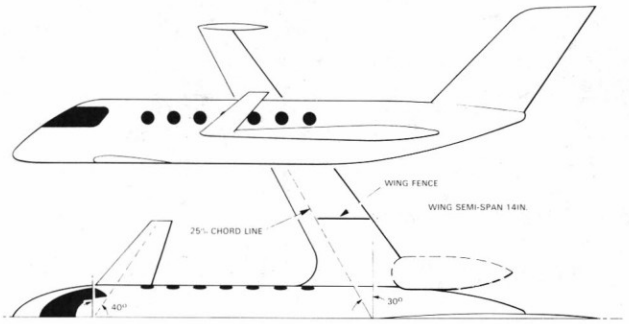

EFSW–CF

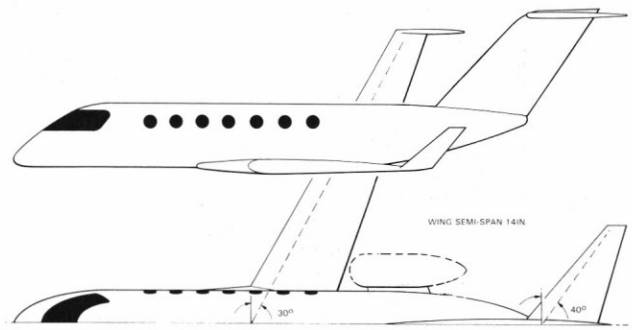

EASW–AT

Fig. 13 "Executive" Type Aircraft Studies

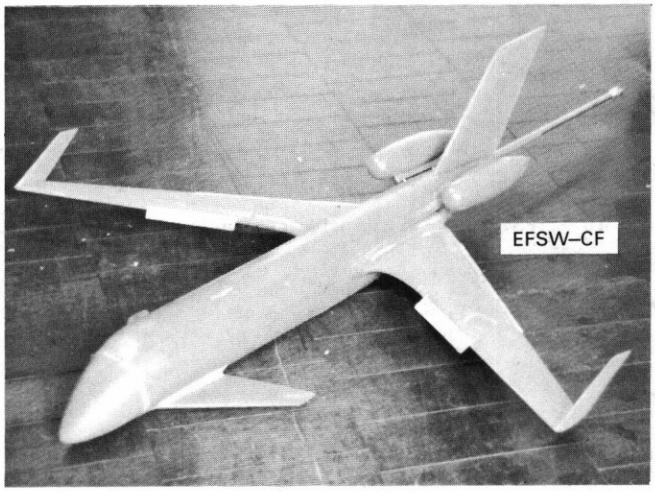

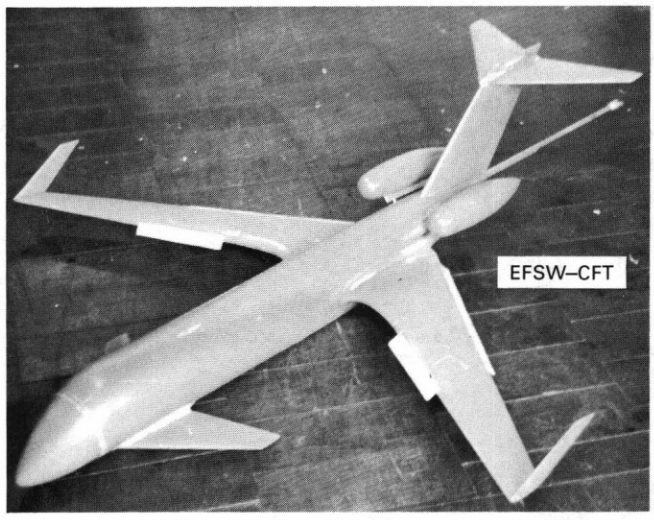

Fig. 14 "Executive" Type Wind Tunnel Models

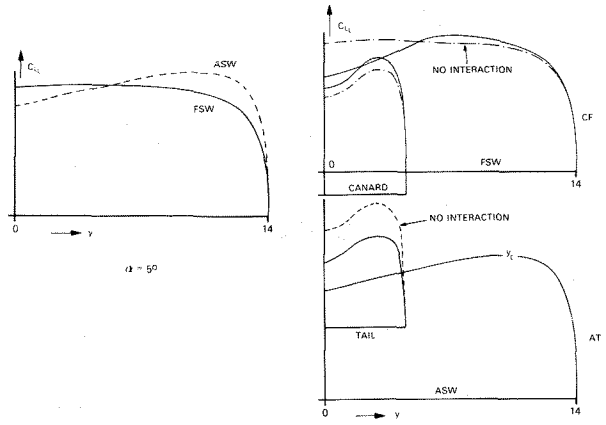

Fig. 15 TFSW & TASW Planar Wing Configurations

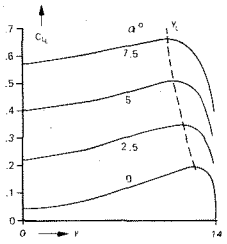

Fig. 16 TFSW with +5° Wing Twist

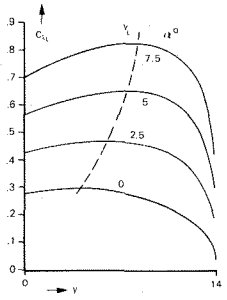

Fig. 17 TASW with –5° Wing Twist

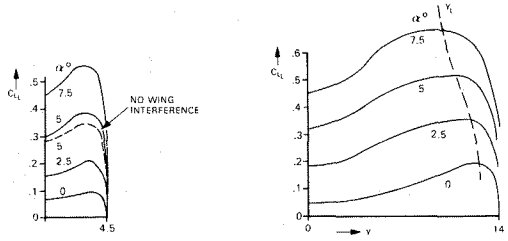

Fig. 18 TFSW – Canard & +5° Twisted Wing

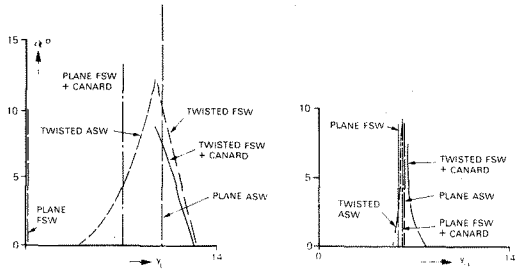

Fig. 19 TFSW & TASW – y_L & y_{cp} Locations

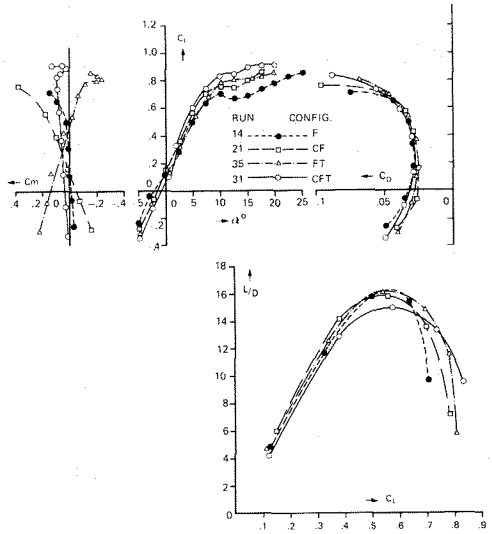

Fig. 20 TFSW – F, CF, FT, CFT Combinations

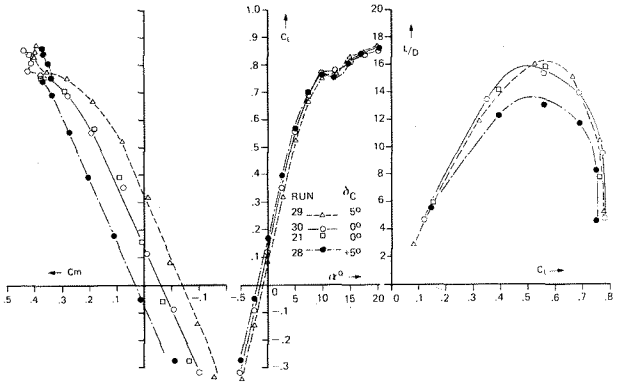

Fig. 21 TFSW – Canard Deflection

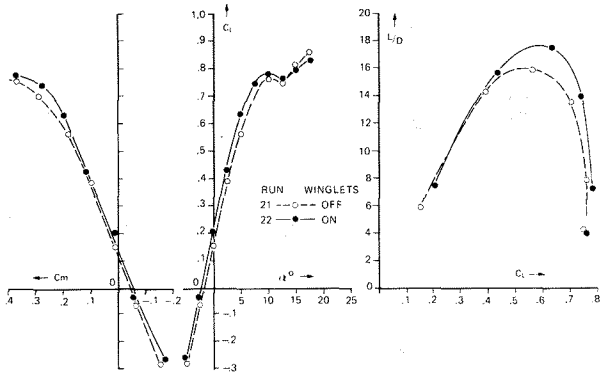

Fig. 22 TFSW – Winglets (CF)

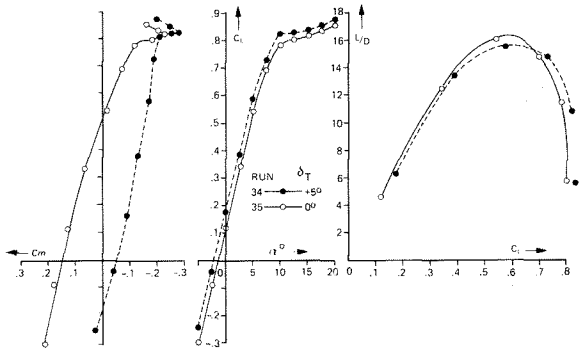

Fig. 23 TFSW – Tailplane Deflection (FT)

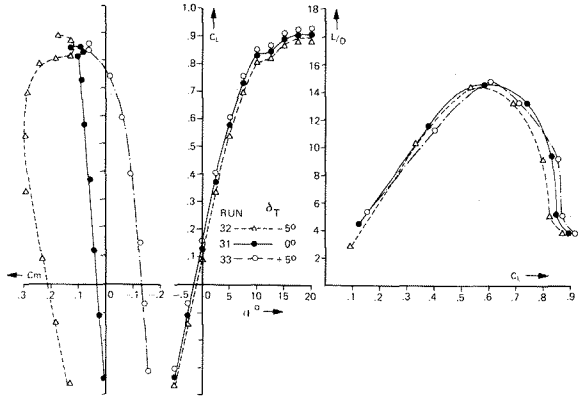

Fig. 24 TFSW – Tailplane Deflection (CFT)

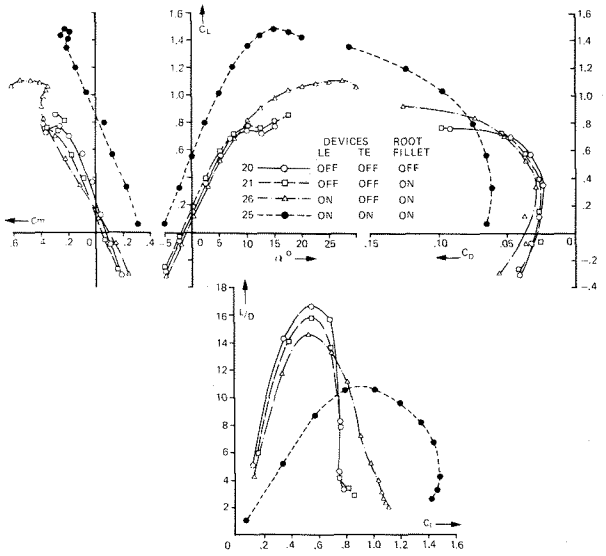

Fig. 25 TFSW – LE Devices on CF

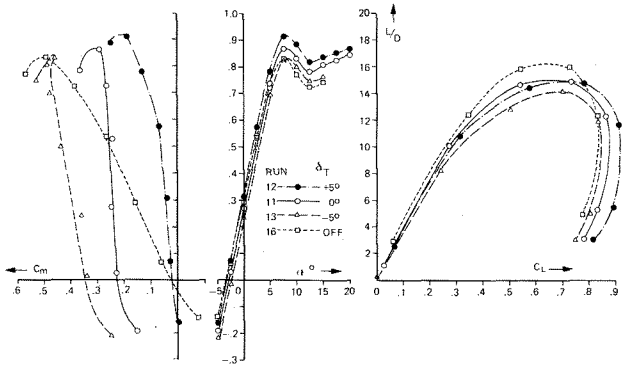

Fig. 26 TASW – Tailplane Deflection

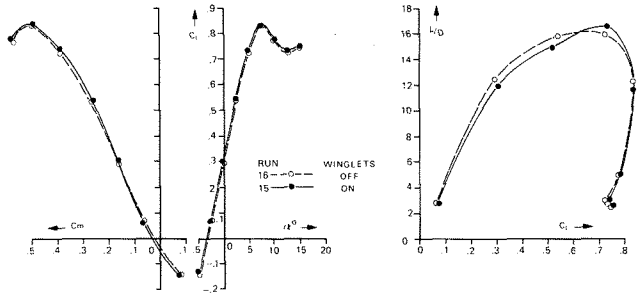

Fig. 27 TASW – Winglets (A)

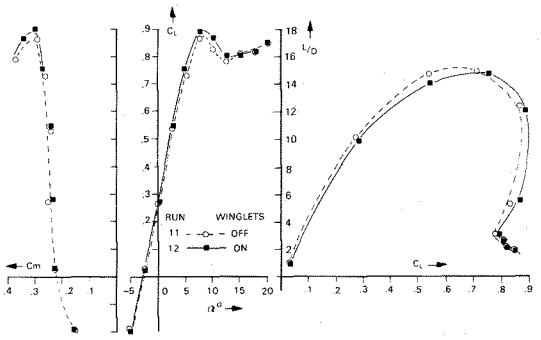

Fig. 28 TASW – Winglets (AT)

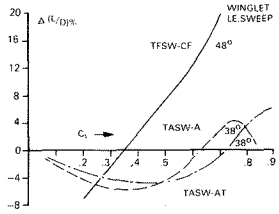

Fig. 29 TFSW & TASW – L/D Improvement due to Winglets

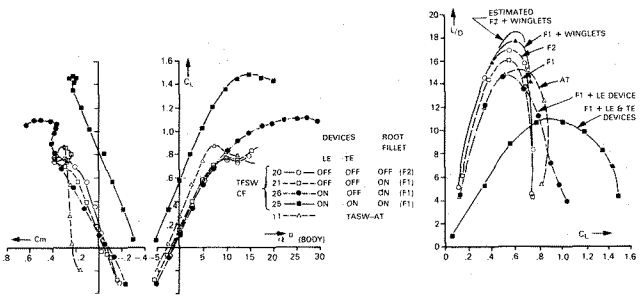

Fig. 30 TFSW & TASW Comparisons

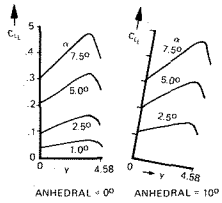

Fig. 31 EFSW & EASW – Trimming Surface–Canard or Tailplane

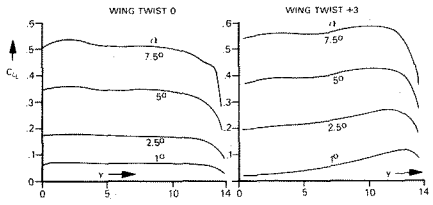

Fig. 32 EFSW – Effect of +3° Twist

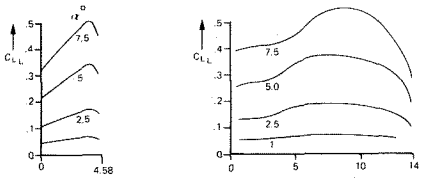

Fig. 33 EFSW – Canard & Plane FSW

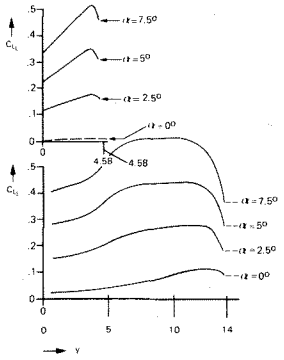

Fig. 34 EFSW – Canard & +3° Twisted FSW

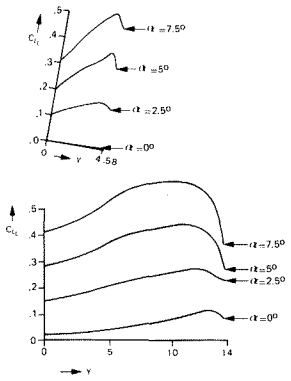

Fig. 35 EFSW – Canard (10° Anhedral) & +3° Twisted FSW

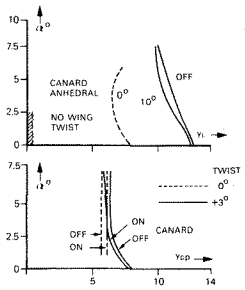

Fig. 36 EFSW – Positions of y_L & y_{Cp}

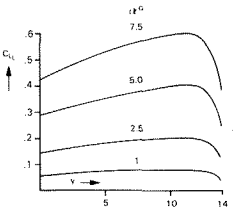

Fig. 37 EASW – No Twist

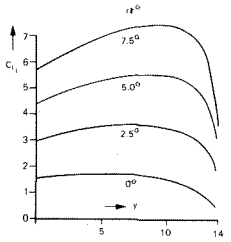

Fig. 38 EASW with –3° Twist

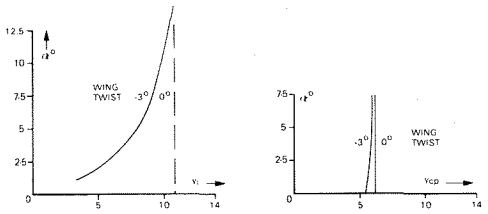

Fig. 39 EASW – Positions of y_L & y_{cp}

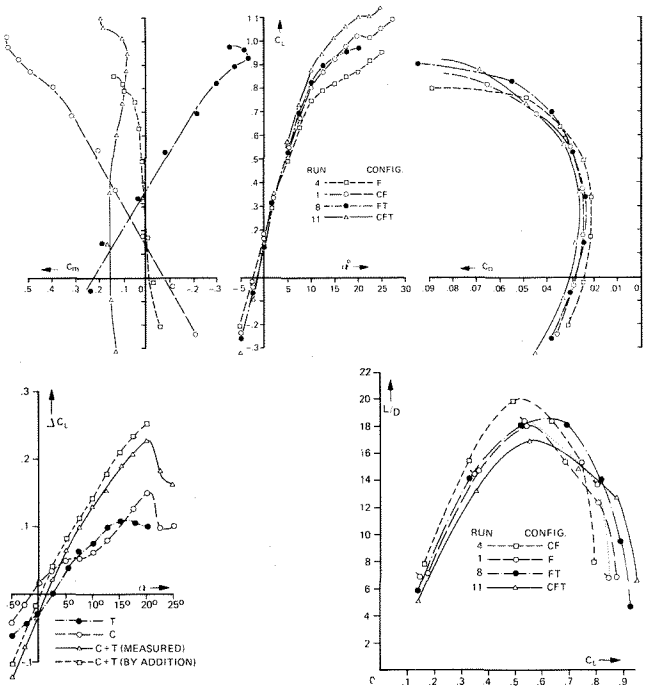

Fig. 40 EFSW–F, CF, FT, CFT Combinations

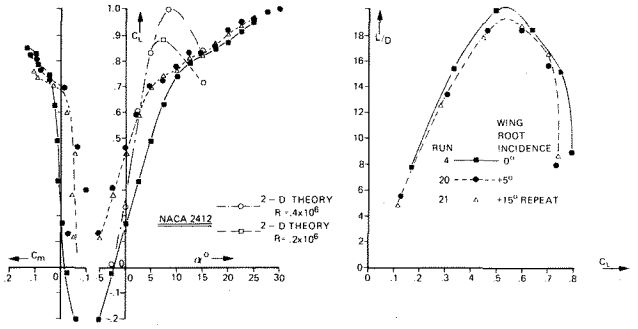

Fig. 41 EFSW–iw Effects on Wing-body (F)

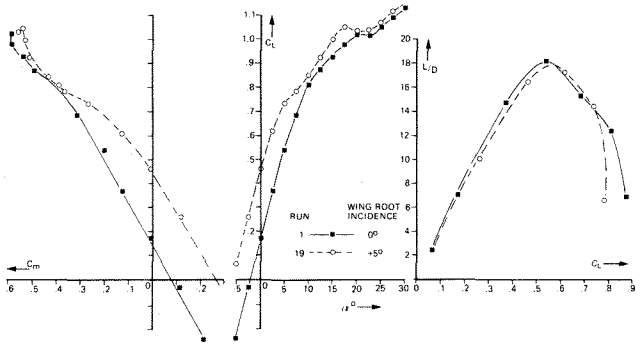

Fig. 42 EFSW–iw Effects on CF

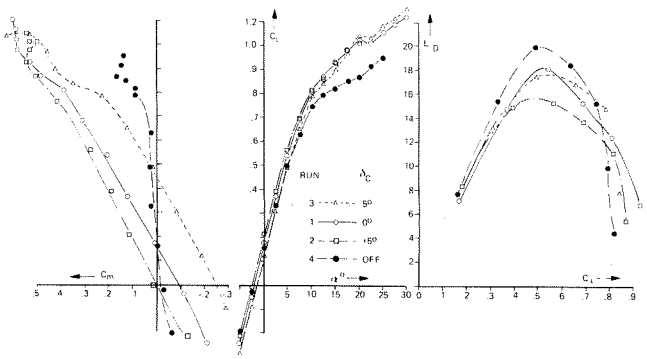

Fig. 43 EFSW – Canard Deflection

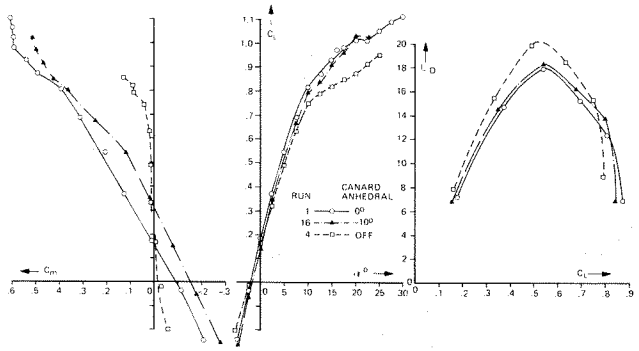

Fig. 44 – EFSW – Canard Anhedral

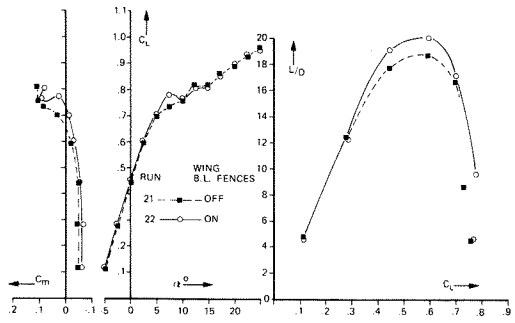

Fig. 45 EFSW – Wing Fences on F

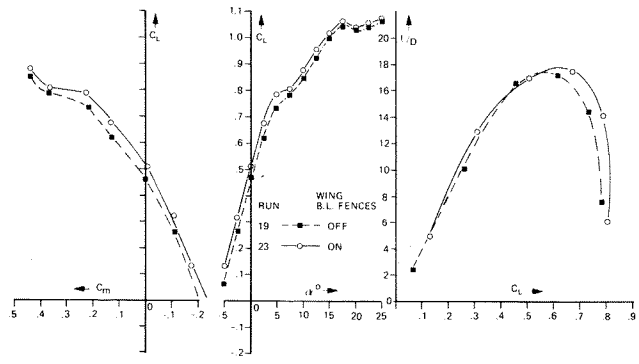

Fig. 46 EFSW – Wing Fences on CF

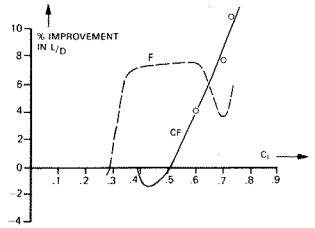

Fig. 47 $L/_D$ Improvements due to Wing Fences

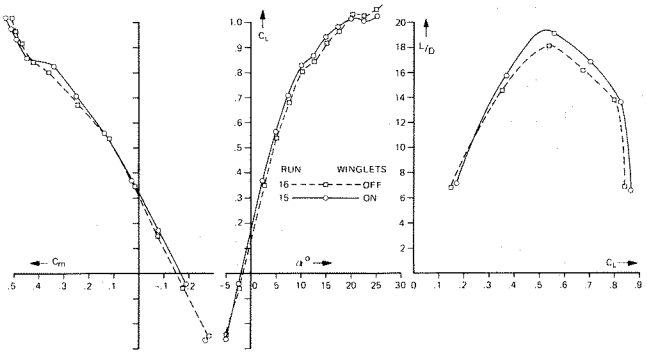

Fig. 48 EFSW – Winglets (CF)

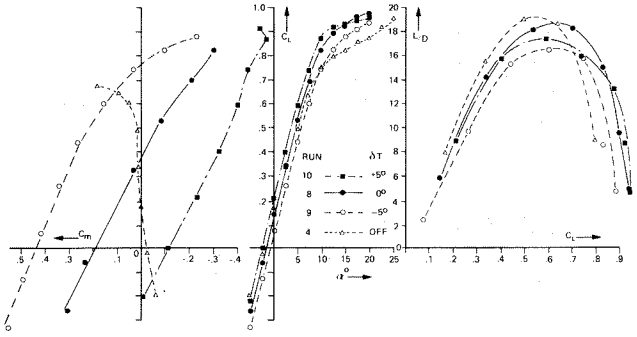

Fig.49 EFSW – Tailplane Deflection (FT)

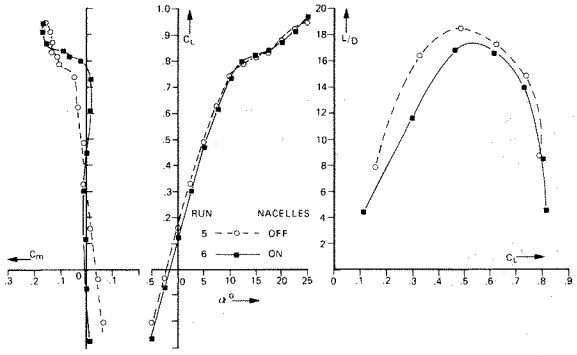

Fig. 50 EFSW – Nacelles on F

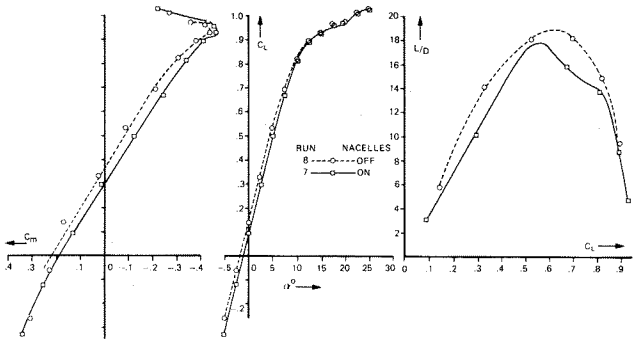

Fig. 51 EFSW – Nacelles on FT

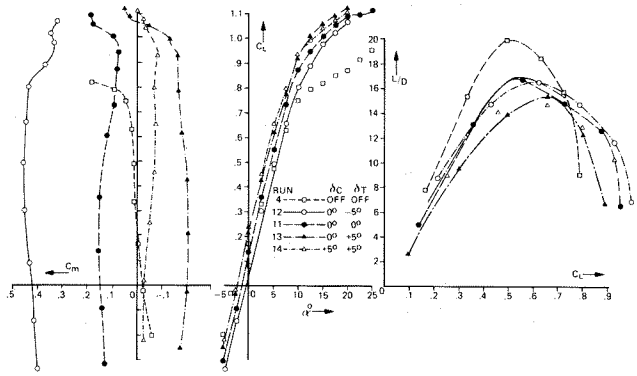

Fig. 52 EFSW – CFT

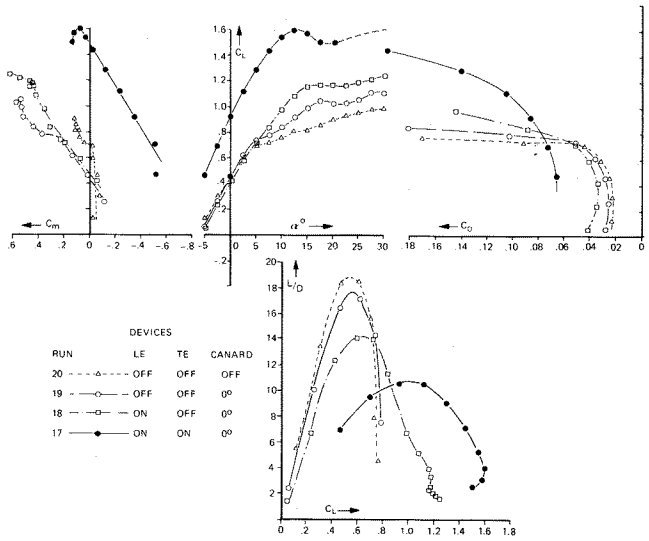

Fig. 53 EFSW – LE & TE Devices on CF

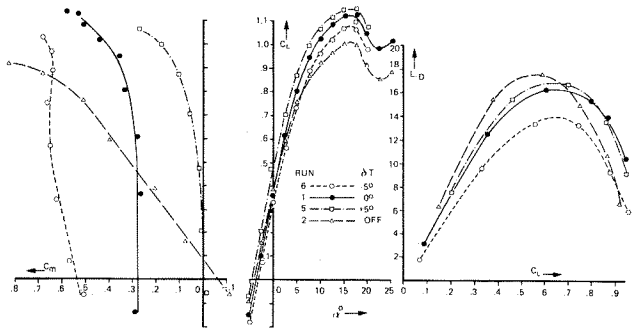

Fig. 54 EASW – Tailplane Deflection

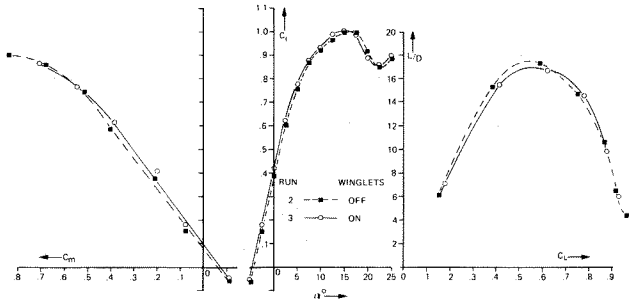

Fig. 55 EASW – Winglets on A

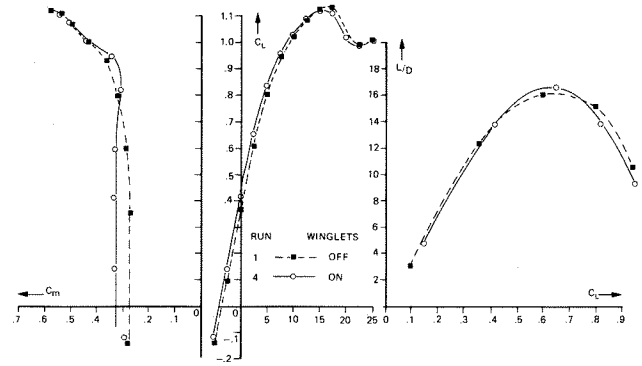

Fig. 56 EASW – Winglets on AT

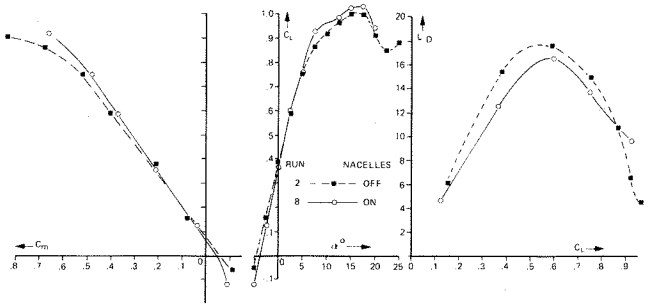

Fig. 57 EASW – Nacelles on A

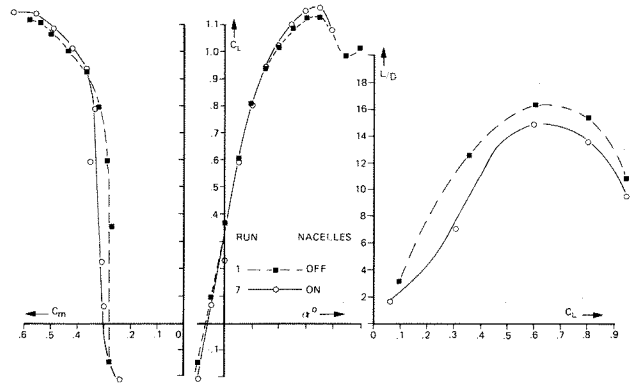

Fig. 58 EASW – Nacelles on AT

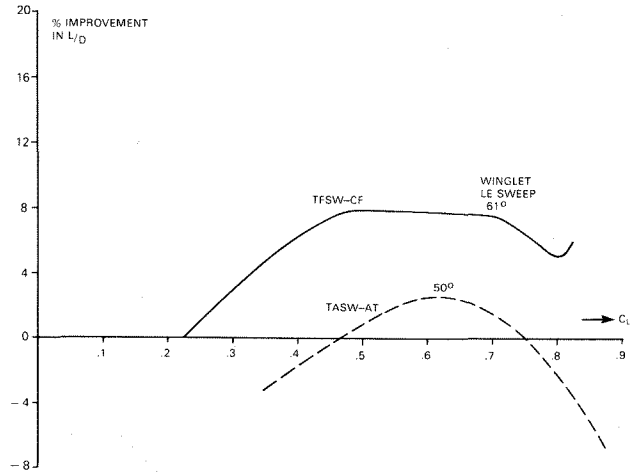

Fig. 59 EFSW & EASW – L/D Improvement due to Winglets

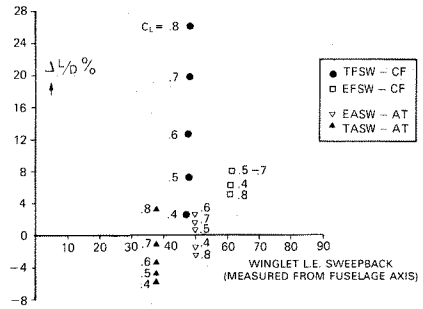

Fig. 60 L/D Improvement and Winglet LE Sweep

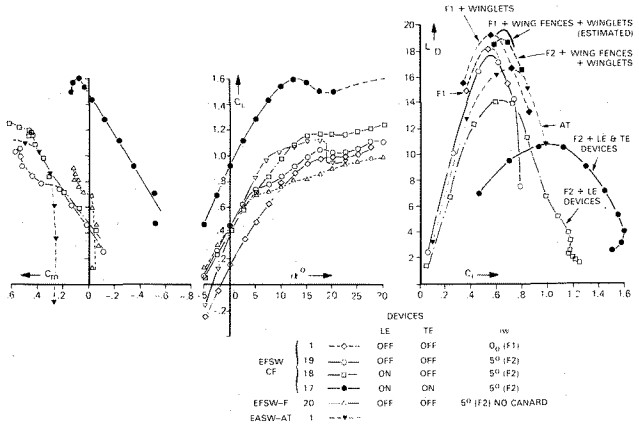

Fig. 61 EFSW & EASW Comparisons

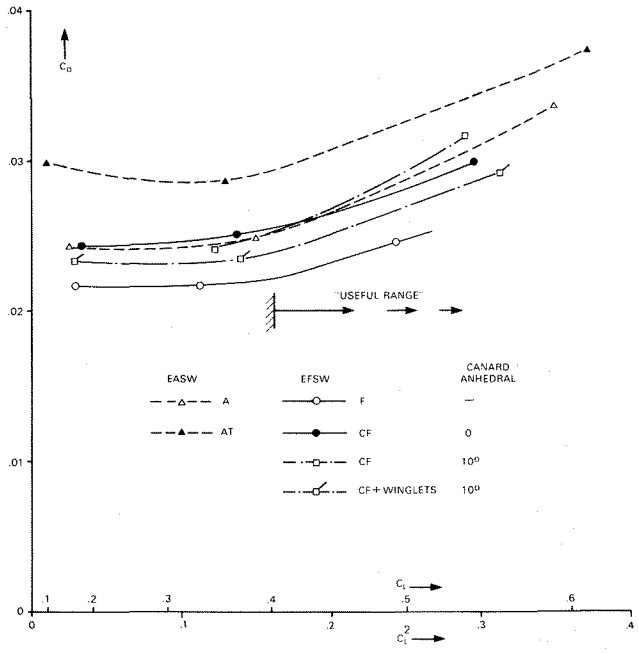

Fig. 62 EFSW & EASW – C_D – C_L^2